Elsevier Editorial System(tm) for Journal of Nuclear Materials
Manuscript Draft

Manuscript Number: JNM-D-11-00546R2

Title: Heavy ion irradiation induced dislocation loops in AREVA's M5 alloy

Article Type: Full Length Article

Corresponding Author: Ms. Rosmarie Martina Hengstler-Eger, Dipl.-Phys.

Corresponding Author's Institution: AREVA NP GmbH

First Author: Rosmarie Martina Hengstler-Eger, Dipl.-Phys.

Order of Authors: Rosmarie Martina Hengstler-Eger, Dipl.-Phys.; Peter Baldo; Ludwig Beck; Joachim Dorner; Karl Ertl; Petra Britt Hoffmann; Christoph Hugenschmidt; Marquis Kirk; Winfried Petry; Philip Pikart; Alexey Rempel

Heavy ion irradiation induced dislocation loops in AREVA's M5® alloy

Cover letter for the second revised submission of the article to the Journal of Nuclear Materials

Pressurized water reactor (PWR) Zr-based alloy structural materials show creep and growth under neutron irradiation as a consequence of the irradiation induced microstructural changes in the alloy. A better scientific understanding of these microstructural processes can improve simulation programs for structural component deformation and simplify the development of advanced deformation resistant alloys. As in-pile irradiation leads to high material activation and requires long irradiation times, the objective of this work was to study whether ion irradiation is an applicable method to simulate typical PWR neutron damage in Zr-based alloys, with AREVA's M5® alloy as reference material. The irradiated specimens were studied by electron backscatter diffraction (EBSD), positron Doppler broadening spectroscopy (DBS) and in-situ transmission electron microscopy (TEM) at different dose levels and temperatures. The irradiation induced microstructure consisted of <a>- and <c>-type dislocation loops with their characteristics corresponding to typical neutron damage in Zr-based alloys; it can thus be concluded that heavy ion irradiation under the chosen conditions is an excellent method to simulate PWR neutron damage.

As recommended by the editor, the abstract has been shortened.

First and corresponding author:

Dipl.-Phys. Rosmarie M. Hengstler-Eger
AREVA NP GmbH
Paul-Gossen-Str. 100
91052 Erlangen
Tel.: +49 (0)9131 900 95337
Cell.: +49 (0)179 4524738
Mail to: Rosmarie.Hengstler-Eger@areva.com

Heavy ion irradiation induced dislocation loops in AREVA's M5® alloy

Detailed Response to the reviewers

The authors want to thank the reviewers for their helpful and detailed comments.

The following changes have been made in the revised article, based on the reviewers' suggestions:

General Changes:

- The units for flux and fluence have been converted from cm^-2 to m^-2.

Reviewer 1:

- The labelling of the sections and subsections in the text has been corrected.
- While a difference in positron lifetime measurements between single vacancies and vacancy clusters can be resolves with positron lifetime measurements, it is more difficult to decide whether the difference would be reflected in the Doppler broadening spectroscopy signal. Therefore, all passages implicating such a correlation have been removed or reworded, as recommended by the reviewer.
- The reference for 0.3wt.% of Nb in solution has been added.
- The references have been re-ordered to appear in the right order.
- A schematic of the EBSD specimen cutting process has not been included; however, the specimen preparation description has been revised to make it more comprehensible.
- The typing error of 6450°C annealing temperature has been corrected.
- The diffraction vector for the <a>-loop observation was (11-20) and not (11-21) as was incorrectly stated in the draft; the error has been corrected.
- The interpretation of the additional reflexes in sample A1 after irradiation has been reworded. A more detailed explanation is given why oxidation is not assumed to be the cause of the changes.
- A lower limit for the size of voids that would be visible under the chosen imaging conditions was added.
- In the description of the <c>-loop linear density calculation, it has been added that this is an established method of loop density quantification and has been used to be able to compare the measured densities with literature data. Loops with diameters larger than the thickness of the foil can not be produced in the experiment as described by this work. The samples are electrolytically thinned before they are being irradiated. Therefore, the size of loops being formed during irradiation is limited by the foil thickness. In studies on neutron irradiated bulk material where TEM foils are being prepared after the irradiation, such large loops might be possible. However, if they are assumed to be distributed homogeneously over the material, some would be observed partly when coming

in from the upper side of the TEM foils while others would be observed partly by going out of the lower side of the foil. Thus, the measured average loop linear density of the foil would not be affected. Loop diameters would be measured too short, though.

Reviewer 2:

- A comment has been added that the <c>-loops, which are generally assumed to be of vacancy-type, are the major microstructural features being studied in this work due to their possible correlation to macrostructural breakaway growth.
- Electron and proton irradiations have been mentioned as suitable simulations for neutron irradiations.
- The repeated passages have been shortened or removed.
- The information about the ZrNb precipitates has been added.
- The reference to MSpec has been added; both the Makhovian function and the data used for the linear interpolation are contained in the already cited paper from Puska and Nieminen.
- The difference in the visible thickness of the irradiated layer in the EBSD plots, which is due to the inclination of the cross-section, has been described in more detail.
- The comment on the depth dependence of the S-parameters of the irradiated sample shown in figure 6 has been adjusted.
- A comment has been added on the possible influence of the second phase on DBS measurements during defect annealing.
- The thickness of grain A1 was not measured due to the high contrast level after the irradiation; its thickness was assumed to be 100nm because of its distance to the hole, which was significantly lower than for grain A2. A comment on this has been added. The typo of 17dpa as the dose level has been corrected in figure 8.
- A comment has been added that <a>-loops are expected to be of both interstitial and vacancy type, but that <a>-loop types could not be investigated experimentally due to their high density and the resulting strong contrasts. There is no reference available in the open literature for the <a>-loop sizes in M5; thus, the respective comment has been removed.
- The hydride observable in the image was a singular hydride and is believed to be a result of a locally high H concentration after electrolytical thinning. It is not representative for the sample condition, as there were no other hydrides present. Thus, an image of another grain has been chosen to avoid misunderstandings.
- A comment has been added that the assumed linear correlation of the <c>-loops' linear density is only valid for the observed dose region, and specifically not for the lower dose region of the <c>-loop formation threshold. As the linear density is zero until that significant dose threshold, it will then rise suddenly before it follows the observed linear curve.
- The captions of the figures describing the irradiation induced microstructure have been changed to contain also the irradiation conditions.

First and corresponding author:

Dipl.-Phys. Rosmarie M. Hengstler-Eger
AREVA NP GmbH
Paul-Gossen-Str. 100
91052 Erlangen
Tel.: +49 (0)9131 900 95337
Cell.: +49 (0)179 4524738
Mail to: Rosmarie.Hengstler-Eger@areva.com

*Manuscript
Click here to view linked References

Heavy ion irradiation induced dislocation loops in AREVA's M5® alloy

R. M. Hengstler-Eger[a], P. Baldo[b], L. Beck[c], J. Dorner[d], K. Ertl[d], P. B. Hoffmann[a], C. Hugenschmidt[e], M. A. Kirk[b], W. Petry[e], P. Pikart[e], A. Rempel[a]

[a]*AREVA, AREVA NP GmbH, Paul-Gossen-Str. 100, 91052 Erlangen - Germany*
[b]*Argonne National Laboratory, Materials Science Division, 9700 South Cass Avenue, 60439 Argonne IL - USA*
[c]*Maier-Leibnitz-Laboratorium (MLL), Am Coulombwall 6, 85748 Garching - Germany*
[d]*Max-Planck-Institut für Plasmaphysik, Boltzmannstr. 2, 85748 Garching - Germany*
[e]*Forschungsneutronenquelle Heinz Maier-Leibnitz (FRM II), Lichtenbergstr. 1, 85747 Garching - Germany*

Abstract

Pressurized water reactor (PWR) Zr-based alloy structural materials show creep and growth under neutron irradiation as a consequence of the irradiation induced microstructural changes in the alloy. A better scientific understanding of these microstructural processes can improve simulation programs for structural component deformation and simplify the development of advanced deformation resistant alloys. As in-pile irradiation leads to high material activation and requires long irradiation times, the objective of this work was to study whether ion irradiation is an applicable method to simulate typical PWR neutron damage in Zr-based alloys, with AREVA's M5® alloy as reference material. The irradiated specimens were studied by electron backscatter diffraction (EBSD), positron Doppler broadening spectroscopy (DBS) and in-situ transmission electron microscopy (TEM) at different dose levels and temperatures. The irradiation induced microstructure consisted of <a>- and <c>-type dislocation loops with their characteristics corresponding to typical neutron damage in Zr-based alloys; it can thus be concluded that heavy ion irradiation under the chosen conditions is an excellent method to simulate PWR neutron damage.

Key words: zirconium-based alloys, ion irradiation, positron spectroscopy, FRM II, positron source NEPOMUC, in-situ TEM, ANL

1. Introduction

Zr-based alloys are used as cladding and structural materials for PWR fuel assemblies due to their low thermal neutron cross section, high melting point and their good mechanical stability and corrosion resistance. However, the alloys experience microstructural degradation due to neutron irradiation which depends not only on neutron flux and fluence but also on parameters like the material's temperature, external and internal stress, hydrogen uptake and corrosion [1]. The neutron irradiation induced microstructure in Zr-based alloys is dominated by a high density of mostly interstitial-type dislocation loops on the hcp lattice's prism planes ("<a>-loops") that are present from low neutron doses and a significantly lower density of vacancy-type dislocation loops ("<c>-loops") on the basal planes whose presence is reported for high neutron fluences only. During irradiation without external stress, these dislocation loop structures are described to lead to a volume conserving expansion along the $\vec{a}$-axes and a contraction along the $\vec{c}$-axis, which is known as irradiation growth [2–10]. For polycrystalline materials, the growth of the single grains can result in a macroscopic structural component deformation, depending on a high number of factors like the material's texture, geometry, grain size, grain boundary properties, second phase precipitate structure and the level of cold work. In nuclear reactor environments, irradiation growth of structural materials occurs in combination with irradiation induced creep, the material deformation under external stress. The onset of the <c>-loop development has been correlated by many authors to the observation of an increase of macroscopic fuel assembly (FA) growth at high fluences ("breakaway growth") [2–6, 8–10]. Therefore, the onset of <c>-loop formation and the <c>-loops' size and density distribution are the major microstructural features being studied in this work.

While the FA components' deformation under standard reactor operating conditions can be predicted, an even higher level of accuracy in the prediction codes, e.g. for the development of new deformation resistant alloys, could be provided by a better scientific understanding of the microstructural processes that cause irradiation induced growth.

Due to the high complexity of the processes leading to macroscopic material growth, such better understanding can be reached by isolating and varying single experimental parameters. This is not possible in a nuclear reactor but can be achieved to a higher degree by simulating neutron irradiation by electron, light or heavy ion irradiation [8, 11–24]. During electron or ion irradiation, experimental parameters can be easily controlled, as compared to a nuclear environment. Also, the irradiation times that lead to typical nuclear power reactor end-of-life doses are low, and an activation of the target material can be avoided; thus, electron and ion irradiation provides simplified sample handling and strongly reduced experimental time and effort. Using a TEM that is combined with an ion accelerator like the IVEM-Tandem Facility of the Argonne National

Laboratory (ANL), in-situ observation of the damage structure development during ion irradiation is possible [25]. The irradiation defect formation and migration can then be observed dynamically which provides a high level of information about the microstructural processes that is impossible to be gained in a nuclear reactor environment. The focus of this study was the simulation of neutron damage with self-ions (Zr) and inert heavy ions similar in mass (Kr), as Zr would be the typical primary knock-on atom species in neutron irradiated Zr-based alloys, and to avoid chemical interaction with the target.
Contrary to neutron irradiation, ion irradiation damage is inhomogeneous over the material depth and follows a peaked profile. To allocate the observed damage level to a specific ion dose, it is thus required to measure either in dependence of the material's depth or to use samples with a thickness that is thin enough to use the ions in transmission; then, the ions interact with the material in the high energy part of the spectrum where the damage levels are approximately homogeneous. Both methods have been used in this work. M5® foil samples irradiated with Zr ions in the low MeV region have been studied depth-dependently by positron Doppler broadening spectroscopy [26–29] at the high intensity monoenergetic positron source NEPOMUC at the German research neutron source FRM II [30–32]. TEM samples with thicknesses in the range of 150 nm have been investigated by in-situ TEM at the ANL's IVEM-Tandem Facility, using Kr ions with 1 MeV in transmission.
To compare the ion doses to typical neutron doses, the displacements per atoms (dpa) were calculated, based on simulations with the SRIM Monte Carlo ion transport code [33]. To verify whether the calculated recoil ranges correspond to the real recoil behaviour in the alloy, the thickness of the damaged layer of a 40 MeV Zr irradiated sample was measured by EBSD.

2. Materials and Methods

2.1. Damage Level Calculations

2.1.1. Ion Irradiation Damage Levels

For the ion induced damage level calculations, SRIM was used in the "detailed calculation with full damage cascades" mode for 1000 projectile ions with the kinetic energies used in the different irradiation experiments [33]. The target is made up of 99 wt.-% Zr and 1 wt.-% Nb with the room temperature density of the alloy of ρ=6.50 g/cm^3. For the 300°C simulations, the target's thermal expansion has been taken into account, which leads to a density of ρ=6.46 g/cm^3. A displacement energy of 40 eV for hcp Zr was chosen, as recommended by G. Was [8]. While only about 0.3 wt.% Nb are dissolved in the Zr matrix at 300°C [34], the remaining 0.7 wt.% Nb are precipitated as bcc ZrNb; thus, based on the recommended displacement energy for bcc Nb, 60 eV [8], a weighted average binding energy of 54 eV has been used for Nb in M5®.
The number of displacements per ion, N_d^{1ion}, and the ion penetration depth d are provided by the SRIM calculations. Then, the damage level D in dpa can be calculated as follows:

$$D = \frac{F \cdot N_d^{1ion} \cdot M_{mol}}{\rho \cdot d \cdot N_A}$$

F is the ion fluence, M_{mol} the target's molar mass of 91.24 g/mol and N_A Avogadro's constant.
For the in-situ ion irradiation, the ions have been used in transmission; d is then the thickness of the electrolytically thinned TEM foil at the position of the observed grain.

2.1.2. Comparison to PWR Neutron Damage Levels

To compare the material damage under ion irradiation to material under PWR neutron irradiation, the fast neutron flux (>1 MeV) typically given for neutron irradiated material data found in the literature has to be converted to dpa. For the neutron irradiation literature data in section "Results", this conversion was done using the method proposed by D. Baron in the frame of an Electric Power Research Institute report in 2009 [35] in cases where the dpa value was not directly given in the reference. The conversion is based on a Zr displacement energy of 40 eV as recommended by G. Was [8], the SPECTER code library based on ENDF/B-5 and a 100 energy group neutron structure. This conversion method for different reactor neutron spectra is reported to be in good agreement with previous literature by V.N. Shishov [36].
Most of the ion irradiated samples were held at 300°C during irradiation, with typical PWR guide tube temperatures being in the range of 300°C to 330°C; thus, the comparability of temperature dependent microstructural processes like defect diffusion and recombination was ensured.

2.2. Sample Preparation and Characterization

The samples studied in this work were cut by laser cutting from polycrystalline M5® industrial strips with thicknesses of 0.38 mm and 0.43 mm. The strips' chemical composition was 0.99 wt.-% Nb, 1350 wt.-ppm O, 17 wt.-ppm S and 98.9 wt.-% Zr. They were produced by subsequent hot and cold rolling of a hot forged alloy slab with an original thickness of 110 mm, with the final heat treatment chosen to fully recrystallize the material. After the foil cutting and sample preparation steps, the samples were vacuum annealed for 2 hours at 580°C to restore an undisturbed recrystallized microstructure. The recrystallized samples show the typical α-Zr hcp lattice structure, an average grain size of 2 to 4 μm and contain spherical bcc ZrNb precipitates with diameters in the range of 30 nm to 50 nm (see Fig. 1). The Nb content of these β-Nb precipitates is 85-90 wt.-% [37, 38].
To study the thickness of the irradiated layer by EBSD, a cross section of an irradiated sample was prepared and analyzed. To assure a good edge retention of the irradiated surface of the specimen, an unirradiated specimen was glued onto the irradiated side of the irradiated specimen; then, both foils were embedded in a hot mounting resin. After grinding and polishing with colloidal silica, the cross section was swab etched with a specific electrolyte. The rounding of the edges of the irradiated foil during cross section grinding parallel to the foil normal showed to be in the range of several μm and thus near the expected irradiated layer's position. Therefore, the cross section was not ground and polished parallel to the foil normal but

with an angle of 35° to the foil normal. As the irradiated layer was thus cut under an angle of 35°, its observable width was increased, improving the depth resolution.
For the low dose irradiation for DBS, the foil specimens' surface was pickled by an hydrofluoric acid based etchant. The foils for the TEM samples were thinned with the same etchant to a thickness of about 100 nm. Then, discs of 3 mm diameter were punched from the foils, and the discs were electrolytically thinned to perforation using a twin-jet electrolytic process at -0°C.
Due to the rolling process, the samples show a very strong texture with the majority of the grains' (0002) $\vec{c}$-axes tilted with an angle of about 25° from the foil surface normal.

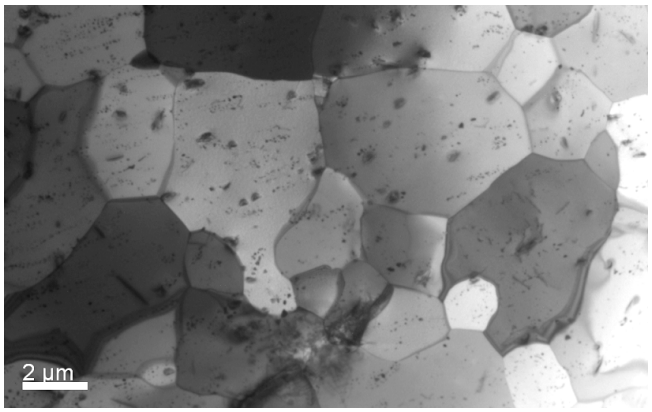

Figure 1: TEM image of M5®'s unirradiated microstructure

2.3. Ion Irradiation

2.3.1. Irradiation at MLL and IPP Accelerators

As a first irradiation test, a M5® sample was irradiated at the MLL tandem accelerator. $^{90}Zr^{4+}$ with 40 MeV was used as projectile to an ion fluence of approximately $3{\cdot}10^{19}m^{-2}$; the sample was held at 300°C during the irradiation. The beam with an average ion flux of $2{\cdot}10^{15}m^{-2}s^{-1}$ was kept continuously on the sample, and the temperature was measured by a Pt-Rh thermocouple spot-welded to the sample's surface directly next to the beamspot area. Due to the ions' inhomogeneous damage profile which is spread to a depth of about 5.5 μm with a damage peak full width half maximum of about 1.2 μm, the damage level was calculated by approximating the irradiated volume as a layer of thickness 1.2 μm with 0.7 of all displacements occurring in that sample region.
Low temperature ion irradiation was done at the tandem accelerator of the Max-Planck-Institute for Plasma Physics (IPP) in Garching, Germany. $^{90}Zr^{1+}$ with 3 MeV and an average ion flux of about $1.9{\cdot}10^{15}m^{-2}s^{-1}$ was used as projectile, to three different ion fluences F. Also, high dose irradiation at 300°C was conducted at the IPP with 2.5 MeV $^{90}Zr^{1+}$. Due to interference of the heating with the ion flux measurement at the IPP sample holder, the damage level at the heated IPP sample IPP-10 is assumed to contain a comparatively high uncertainty in the range of 10%. The ion beam with a beam diameter of about 1 mm was scanned continuously over the samples, thus providing a homogeneously irradiated beamspot area and avoiding local overheating of the samples. Target temperatures were measured by thermocouples pressed against the samples; the temperature measurement error is estimated to be 5 K for room temperature and 10 K for measurements at 300°C.
The irradiation parameters for the samples at the MLL and IPP accelerators are summarized in Table 1; E_{ion} is the ions' energy, F_{ion} the ions' fluence, D_{dpa} is the total damage level and $\dot{D}_{dpa}$ the damage rate.

2.3.2. Irradiation at the ANL's IVEM-Tandem Facility

At the ANL's IVEM-Tandem Facility, three electrolytically thinned TEM samples were irradiated with 1 MeV Kr^{++} ions with an ion flux of $6.25 \cdot 10^{15}m^{-2}s^{-1}$. The beam was rastered over the TEM samples to provide a homogeneous ion fluence on all sample regions. The beamline of the ion accelerator is directly interfaced with a Hitachi H9000 300 keV TEM where the samples are positioned with an initial angle of 30° to the ion beam, thus allowing in-situ observation and imaging of the samples during irradiation. The samples were held at 300°C by a Gatan two-angle tilt heating stage. With sample thicknesses in the imaged regions in the range of 150 nm, the ions were used in transmission. Calculations with the SRIM Monte Carlo code show a transmission of the incident ions of 90% for a sample thickness of 150 nm. The Kr ions in transmission produce the displacements in the TEM samples while still in their high energy regime, thus creating an approximately homogeneous damage distribution through the material. As all defects are viewed in their two dimensional projection in the TEM images, a homogeneous recoil distribution over the sample depth is a major point to produce reliable results.
In sample A1, a grain oriented with the $\vec{c}$-axis perpendicular to the surface was imaged with diffraction vector $\vec{g} = (11\bar{2}0)$ or equivalent with the foil tilted about 10° from the [0001] zone axis in bright field and $(\vec{g}, 3\vec{g})$ dark field conditions. While <c>-component dislocations with Burgers vectors [0001] are invisible under the chosen diffraction condition, all perfect <a>-component dislocation loops with Burgers vectors $[1\bar{2}10]$, $[\bar{1}2\bar{1}0]$ and $[2\bar{1}\bar{1}0]$ are visible, as well as mixed <c+a>-types: [1123], $[\bar{1}2\bar{1}3]$, $[\bar{2}113]$, $[11\bar{2}3]$, $[\bar{1}2\bar{1}\bar{3}]$ and $[\bar{2}11\bar{3}]$ [4]. In sample A2, a grain with the $\vec{c}$-axis parallel to the foil surface was observed in bright field, $(\vec{g}, 3\vec{g})$ and $(\vec{g}, 4\vec{g})$ dark field conditions, using the $\vec{g} = (0002)$ diffraction vector, with the grain tilted approximately 10° from the $[2\bar{1}\bar{1}0]$ zone axis. These diffraction conditions show all <c>-type and <c+a>-type contrasts while suppressing pure <a>-component contrasts [4]. A third sample, A3, was irradiated while being imaged in the same diffraction condition as sample A2; sample A3 contained 110 wt.-ppm hydrogen due to an initially different testing purpose. After irradiation, the <c>-loops' development in that sample was observed while the sample was heated from 300°C up to 750°C.
As the samples were in the TEM during ion irradiation, images could be taken continuously with increasing damage levels. The samples' final ion damage levels are summarized

in Table 2. As the number of recoils produced in the TEM samples depends on the irradiated grains' thickness, the dpa rates are different for the three samples despite the same ion flux. The irradiation parameters for the ANL IVEM-Tandem Facility experiments are shown in Table 2.

Sample	T_{irr}	E_{ion}	F_{ion}	D_{dpa}	$\dot{D}_{dpa}$
MLL	300	40	$3{\cdot}10^{19}$	21	10
IPP1	35	3	$2.5{\cdot}10^{17}$	0.1	7
IPP2	35	3	$5{\cdot}10^{17}$	0.2	7
IPP3	35	3	$1{\cdot}10^{18}$	0.4	7
IPP-10	300	2.5	$4{\cdot}10^{19}$	16	7

Table 1: Irradiation parameters for samples irradiated at MLL and IPP accelerators; T_{irr} in °C, E_{ion} in MeV, F_{ion} in m^{-2}, $\dot{D}_{dpa}$ in 10^{-4}dpa/s

Sample	T_{irr}	E_{ion}	F_{ion}	D_{dpa}	$\dot{D}_{dpa}$
A1	300	1.0	$5.0{\cdot}10^{19}$	18	22
A2	300	1.0	$5.0{\cdot}10^{19}$	22	27
A3	300	1.0	$6.3{\cdot}10^{19}$	27	27

Table 2: Irradiation parameters for the samples irradiated at ANL's IVEM-Tandem Facility; T_{irr} in °C, E_{ion} in MeV, F_{ion} in m^{-2}, $\dot{D}_{dpa}$ in 10^{-4}dpa/s

2.3.3. Electron Backscatter Diffraction

The displacement of target atoms by neutron and heavy ion irradiation leads to a defect microstructure consisting of interstitials ("i"), vacancies ("v"), i- and v-clusters and dislocation loops. The elastic strain in the irradiated alloy's lattice caused by these microstructural features can be studied by EBSD. The normalized sum of the band slope parameter has been used for this study; the band slope (BS) is a numerical image quality parameter that measures the maximum intensity gradient at the seams of the Kikuchi bands. The Kikuchi bands are caused by Bragg diffraction of divergent, incoherent electrons scattered within the specimen; thus, their intensity depends on the crystal lattice periodicity and is lowered by dislocations and their elastic strain fields, which is reflected in the band slope. The band slope parameter can therefore be used to distinguish the irradiated, strongly strained layer from the unirradiated bulk material [39, 40]. The EBSD measurement error of the width of the damaged layer is assumed to be about 5%, resulting from the measuring uncertainty of the angle between foil surface and cross section surface. A Zeiss Neon 40 EsB scanning electron microscope with a Nordlys EBSD camera has been used for the analysis.

2.4. Positron Doppler Broadening Spectroscopy

The high-flux positron source NEPOMUC at the German research neutron source FRM II provides a monoenergetic positron beam of 1 keV in the primary beam and a moderated positron intensity of up to $9 \cdot 10^8 e^+ s^{-1}$ [41]. By applying an electric potential to the sample, the beam's energy can be varied from 0.2 to 30 keV [42]. For Doppler broadening spectroscopy, the electron-positron annihilation gamma energy shift due to the electrons' momentum is measured by up to four liquid nitrogen cooled high purity Ge-detectors with an energy resolution between 0.25 and 0.3% at 511 keV. All measurements have been taken with an integration time of 60 s. DBS experiments use the so-called "S-parameter" as a measure for the vacancy-type defect density in the studied samples. The S-parameter is defined as the 511 keV γ-intensity within a previously defined energy band around 511 keV divided by the total peak intensity and thus reflects the annihilations with low-momentum, i.e. valence or conduction band electrons. In vacancies, the relative probability of positron annihilation with core electrons is lower than in the perfect lattice due to the absence of lattice atoms at the vacancy positions. Thus, for a high vacancy concentration, the higher fraction of annihilations with low-momentum electrons leads to an increase of the S-parameter. The parameter is calculated after the subtraction of the background. As the energy range limits around the 511 keV peak for the S-parameter are defined differently for each material and measurement setup to receive the highest possible resolution, absolute S-parameters can only be compared for samples measured with the same energy window in the same measurement campaign.
The annihilation spectra were analyzed with MSpec 2 [43]; the received S-parameters from the up to four detectors were averaged. Two different measurement types were used: lateral sample scans at fixed positron energy and depth scans at fixed beam position with varying positron energy. The mean positron penetration depth for Zr-based alloys was calculated using the Makhovian function, with the function parameters for Zr calculated by linear interpolation between the parameters for Cu and Ag reported by Puska and Nieminen [44]; for the material density, the mass density of M5® was used.

3. Results and Discussion

3.1. Electron Backscatter Diffraction (EBSD)

For the verification of the SRIM ion penetration depth calculations, a cross-section was prepared from sample MLL. A total length of 330 μm along the irradiated and the unirradiated surface was analyzed with EBSD; the band slope distribution was averaged over the measured length. Figure 2 shows the band slope mapping over the irradiated layer and the unirradiated bulk material near the surface; Figure 3 gives the distribution of the normalized sum of the band slope parameter measured from the specimens' surface to the unirradiated bulk, compared to the recoil distribution calculated with SRIM for 100 ^{90}Zr projectiles with 40 MeV on the alloy. As the cross-section was polished with an angle of about 35° to the foil normal, the cut through the irradiated layer is inclined. Therefore, the EBSD image in Fig. 2 shows an enhanced thickness of the irradiated layer. The BS parameters given in Fig. 3 have been corrected for the cross-section inclination and thus provide the actual thickness of the irradiated layer.

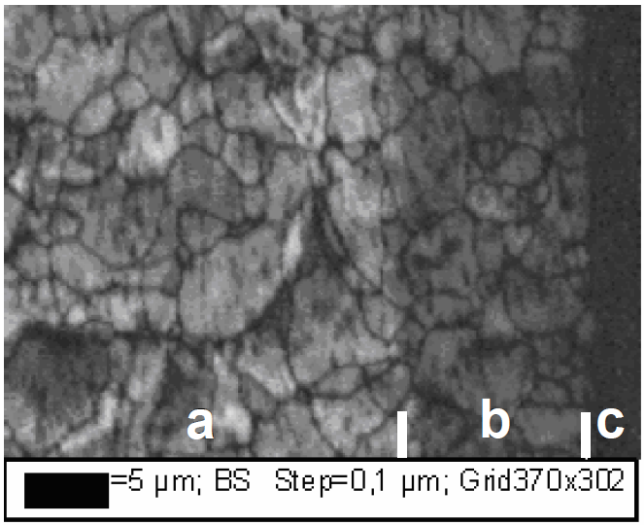

Figure 2: Band slope map of the irradiated specimen (Z40 MeV Zr at 300°C) cut under 35°; a=unirradiated bulk; b=irradiated layer; c=gap to the stabilizing foil

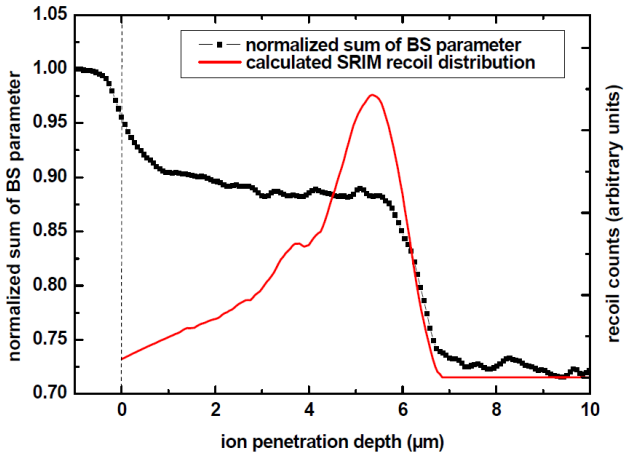

Figure 3: Depth dependent normalized sum of the band slope (BS) parameter compared to SRIM calculation results

The irradiated layer can be clearly distinguished by its darker colouring from the bulk in the band slope map (see Fig. 2). Also, the width of the irradiated layer is approximately constant along the specimen. This shows that, even though the material is hexagonal and might thus be expected to be prone to channeling effects that are disregarded by the SRIM code, channeling does not occur to a significant level, and the damage range does not depend on the grain orientation.

The peaked recoil distribution which was calculated with SRIM is not reflected in the depth dependent distribution of the normalized sum of the BS parameter (see Fig. 3); the sum is approximately constant over the total irradiated layer. This is assumed to be an effect of saturation: as also observed during the in-situ-TEM ion irradiation, the Kikuchi lines become invisible in the TEM in specimens irradiated to high doses due to the high density of defect structures that disturb the lattice planes' periodicity. From the EBSD results, that effect can be assumed to occur already at the comparatively low recoil densities as they are given on the material's surface. Then, the higher recoil density and subsequent higher defect density can not be resolved by EBSD as the Kikuchi lines are already completely dark at the much lower dose.

The damage level at which the saturation occurs has to be lower than the damage level at the specimen's surface, otherwise a part of the peak would be seen in the EBSD signal. The SRIM calculated surface recoil density is about 6% of the peak recoil density. It can thus be concluded that EBSD saturation is reached for recoil densities of 6% of the peak density or lower in the irradiated sample. For the chosen irradiation conditions, and assuming that 70% of the recoils are concentrated in the recoil peak with a full width half maximum of 1.2 μm, the peak damage level is 21 dpa. Then, the calculated damage level at the sample's surface is 1.3 dpa, which can be regarded as the upper limit for EBSD saturation under the chosen measurement conditions.

The measured maximal damage range corresponds very well to the calculated maximum range; it can thus be concluded that the SRIM calculations for heavy ion ranges in M5® produce very realistic results and can be used as a basis for damage level calculations in the specimens with a level of accuracy that is significantly higher than the typical measurement errors in the irradiation experiments.

3.2. Positron Doppler Broadening Spectroscopy

3.2.1. Irradiation at 35°C

Four samples (IPP1, IPP2, IPP3 and an unirradiated standard sample) were scanned depth dependently with a positron energy range from 1 keV to 12 keV, which corresponds to a mean positron implantation depth of 9 nm to 280 nm. The according depth-dependent S-parameters are given in Figure 4. The S-parameters are normalized, i.e. divided by the unirradiated standard's S-parameter for the bulk region; the standard S-parameter is calculated by averaging over the three values measured for the bulk reproducing values at highest positron energies, designated in red.

The S-parameter depth profile for the unirradiated standard in Fig. 4 shows a slight buckling for positron energies between 1 keV and 4 keV before reaching an approximately constant value. This is due to deviations from the material's bulk microstructure near the surface and positrons being scattered back to the surface; for energies higher than 4 keV, surface effects can thus be neglected.

The irradiated samples show an S-parameter about 6% higher than in the unirradiated sample, indicating a high density of vacancy-type defects in the samples. Despite the different damage levels of 0.1 dpa, 0.2 dpa and 0.4 dpa, the three irradiated samples do not show a significant difference in the S-parameter slope near the surface and reach a comparable S-parameter level in the bulk region of the sample. Thus, it can be concluded that the vacancy-type defect density after 35°C Zr ion irradiation is not dependent on the ion dose in the measured low damage

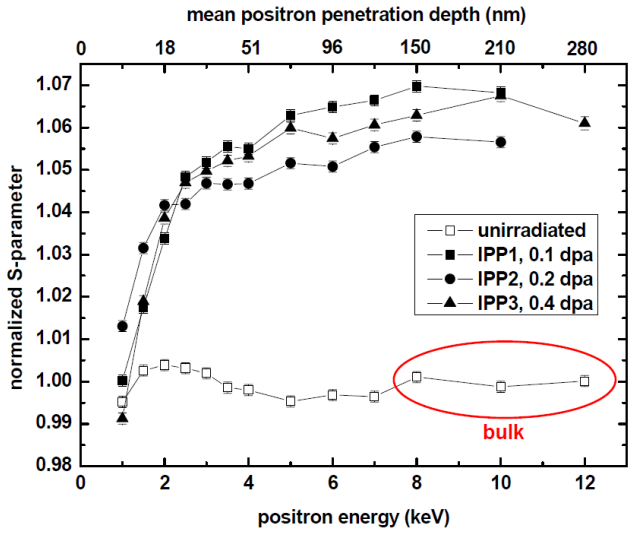

Figure 4: S-parameter depth profile of irradiated M5 (3 MeV Zr at 35°C)

level range. It can therefore be assumed that, under the chosen irradiation conditions and dose range, an equilibrium between vacancy-type defect production and recombination is given.
Sample IPP1 with a total damage level of 0.1 dpa was scanned depth-dependently along a line on the surface leading from the unirradiated to the irradiated layer, thus measuring S(x,E) (see Fig. 5). The step size in x-direction was 0.5 mm, the positron energy step size between 0.5 keV and 1.5 keV. The S-parameter is normalized, using the average of the unirradiated bulk region, 0.530, as unirradiated standard parameter.

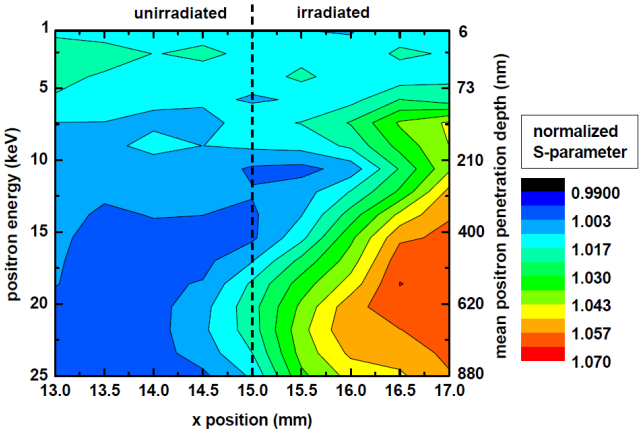

Figure 5: Normalized S-parameter as function of positron energy (depth) and position x

The unirradiated material to the left of the beamspot has a S-parameter corresponding to the S-parameter of the unirradiated standard (see Fig. 4), showing that sample handling before and after irradiation has not induced, e.g. by application of stress, any defects observable by DBS. The observed material changes in the irradiated regions are therefore solely caused by the ion irradiation. The irradiated material in the superficial material region has the same S-parameter as the unirradiated material region, even though according to the SRIM calculations there should be a considerable recoil creation rate also near the surface. A possible explanation is that defects from this superficial layer annihilate at surface sinks or impurities that are present with a higher probability near the surface. In deeper material regions, the observed vacancy-type defect density shows a peaked profile as is to be expected from the SRIM calculations. However, the irradiated volume has a lower S-parameter at the border of the beamspot, located at x=15 mm. Especially for lower penetration depths, the S-parameter increases only slowly with the x position, in the direction of the beamspot center. The general region of S-parameter gradient around the irradiated material volume can be partly due to the stepwidth of 0.5 mm, leading to an averaging of the measurements of unirradiated and irradiated material. However, the irradiated region is broader for higher penetration depths. In the damage peak region the defect formation rate is higher compared to the surface region, where the ion-target interaction probability is lower. For this reason, a possible explanation would be a different production to recombination ratio of defects at higher penetration depths.

3.2.2. Irradiation at 300°C

Fig. 6 shows S-parameter depth profiles of the unirradiated and irradiated sample IPP-10 in combination with the calculated SRIM recoil production profile; the sample was irradiated to a damage level of 16 dpa with 2.5 MeV $^{90}Zr^{+}$. The S-parameters are normalized, using the average of the unirradiated parameters at the three highest energies as standard, as designated in blue.

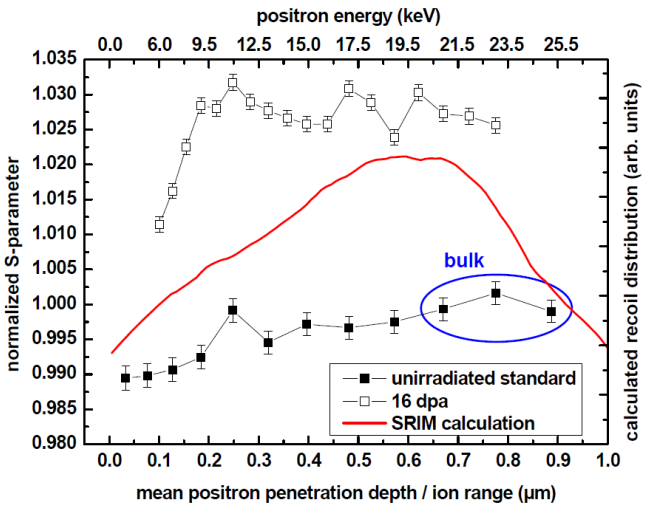

Figure 6: S-parameter depth profile of sample IPP-10 (2.5 MeV Zr at 300°C), observed at room temperature

The irradiated sample shows a significantly higher S-parameter than the unirradiated sample. However, the difference between irradiated and unirradiated material is in the range

of about 2%, while it was about 6% for the samples irradiated at 35°C to significantly lower doses. It can be concluded that a high fraction of the initially created vacancy-type defects in the ion induced recoil cascades are subject to recombination and annihilation at 300°C. This is in accordance with the annealing stages for irradiation induced defects in single-crystal zirconium, as they are proposed by G.M. Hood and W. Frank [2, 45].

According to Hood's interpretation of measurements of electron irradiation induced defect annealing in single crystal pure Zr, the onset of free vacancy migration in α-Zr occurs between -23°C and +27°C [45]. W. Frank's interpretation of the annealing measurements predicts the onset of free vacancy migration to be at around 30°C [2], while he proposes self-interstitials to undergo long-range migration in the annealing stages I and III, with the higher temperature limit of stage III being around 30°C. This suggests that free vacancy migration is possible in the samples irradiated at 35°C only within certain limits, while it can be expected to be a significantly stronger effect at 300°C. Free vacancy migration can thus be assumed to be responsible for the significantly lower vacancy-type defect density in the samples irradiated at high temperature. After the initial increase between the surface and 0.25 μm, the measured S-parameters do not rise further (see Fig. 6), showing that the measured values are representative for the bulk material.

As DBS gives a measure of the vacancy-type defect density only and does not contain information about the defect being in mono-vacancy, cluster or loop form, it is not possible to decide from the DBS measurements alone whether the observed vacancies are in the form of loops or in which crystal planes the loops are located. To test which kind of dislocation loops can be resolved by DBS, the defects in sample IPP-10 irradiated at IPP were annealed during in-situ DBS to image the S-parameter's development with the temperature and to compare the observed annealing effects with dislocation loop imaging during in-situ defect annealing in the TEM. A positron energy of 15 keV was used, which leads to a positron implantation profile clearly located in the bulk region of the irradiated sample, see Fig. 6. The sample was heated from 230°C to 600°C, in steps of about 25°C. The dwell time at each temperature level was 15 minutes, the heating rate between the steps about 9 K/min. During the holding at the different temperature levels, the S-parameters remained constant within the measurement accuracy. The measured S-parameter as a function of temperature, normalized to the S-value of the annealed sample (T=450°C) is shown in Figure 7, in comparison to the annealing curve for single crystal Zr after 1.2 MeV electron irradiation at 120 K as reported by G.M Hood [45]. The annealing stages as suggested by W. Frank [2] are given in the plot.

As expected, the measured S-parameter remains constant between 230°C and 285°C; this confirms the irradiation temperature of the sample to have been higher than 285°C, as all diffusion processes up to that temperature range can be expected to have already taken place during irradiation. From 285°C to 400°C, the S-parameter decreases linearly before it approximates its lowest level at about 450°C, which corresponds to the S-parameter measured for the unirradiated sample. The small

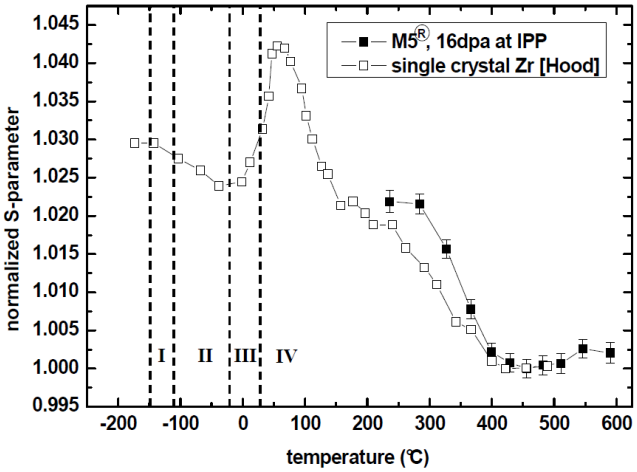

Figure 7: Defect annealing in IPP-10 (irradiated with 2.5 MeV Zr at 300°C), observed with in-situ DBS; comparison to literature data by Hood et al. [45]

increase of the S-parameter for temperatures higher than 450°C is caused by the thermal lattice expansion. While the normalized S-parameter's difference between irradiated and unirradiated state, which depends on the electron or ion implantation fluence and the irradiation temperature, is higher for the measured sample, the curve's lowest point is in very good agreement with the Zr single crystal values provided by G.M. Hood. As electron irradiation is expected not to form recoil cascades but Frenkel pairs only [8] and vacancy migration at 120 K is assumed to be strongly limited at the irradiation temperature of 120 K, the single crystal vacancy-type defect structure can be assumed to consist of mainly mono-vacancies. The corresponding annealing behaviour for sample IPP-10 can be an indication of the dominating defect structures in sample IPP-10. The sample could either host mostly mono-vacancies or it could contain defect loops or clusters with the same annealing characteristics as mono-vacancies. Further studies of the defect annealing behaviour were done by in-situ TEM annealing, as described below.

It is assumed by the authors that the DBS measurements of the S-parameters during annealing are unaffected by possible changes in the second phase particles. Changes in these particles with regard to size, number, distribution or crystallinity were not observed during additional studies with the TEM. Also, the total second phase particle volume as compared to the measured sample volume is low. Finally, the temperature increase was done relatively fast; it is thus not expected to trigger measureable shifts in the phase distribution.

3.3. In-situ TEM

3.3.1. <a>-Component Dislocations

The development of <a>-component dislocation loops has been observed in one grain of sample A1 from the unirradiated state to an ion fluence of $5.0 \cdot 10^{19} \mathrm{m}^{-2}$. The grain's thickness was not measured; to estimate the ion dose, a thickness of 100 nm was assumed, based on the grain's distance from the

hole. This leads to a calculated maximal ion dose of 17 dpa. As soon as the irradiation was started, small <a>-loop contrasts started to develop and to migrate in the grain; their density increased with the dose (see Fig. 8). Fig. 9 shows the <a>-loop contrast in higher magnification; contrasts of loop form are designated by the arrows.

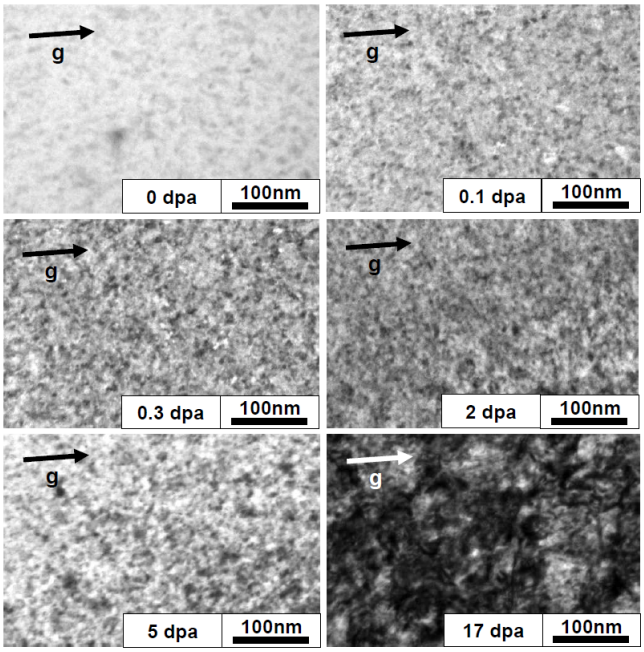

Figure 8: <a>-loop development vs. ion dose (1 MeV Kr at 300°C); $\vec{g} = (11\bar{2}0)$ or equivalent

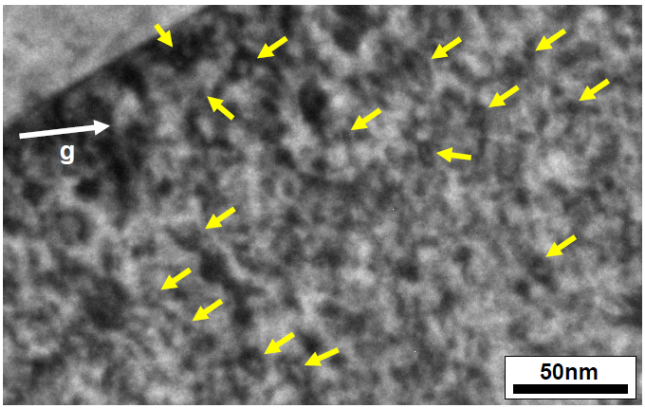

Figure 9: <a>-loop contrast in higher magnification (1 MeV Kr at 300°C); $\vec{g} = (11\bar{2}0)$ or equivalent

At the maximum dose of 17 dpa, the <a>-component dislocation network shows regions of very dense contrasts alternating with lower contrast regions. The [0001] zone axis diffraction pattern after 17 dpa shows significant deviations from the lower dose state (see Fig. 10): while the initial hexagonal diffraction pattern is barely recognizable, additional reflexes are present. They might be assumed to be an indication of recrystallization of grain regions into small grains with a slight deviation of orientation or lattice parameters from the original grain. This recrystallization could be a consequence of very strong bending of the grain in combination to the high defect density, as it was observed in a grain close to the hole at high damage levels. Oxidation as a cause for the observed changes in the images and diffraction pattern is deemed unlikely because comparable samples have not shown the observed effects, neither while being irradiated at corresponding pressure and ion dose conditions, nor during annealing experiments at up to 750°C.

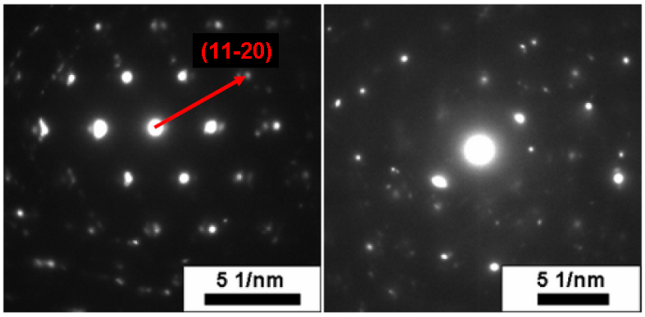

Figure 10: [0001] zone axis diffraction pattern at 0 dpa and 17 dpa (1 MeV Kr at 300°C)

The <a>-loop contrast size distribution has been measured at ion doses 0.3 dpa, 1 dpa and 2 dpa (see Fig. 11); for higher doses, the high contrast density prohibited reliable measurements. The <a>-loops' size distribution shows only a slight increase with the dose. The <a>-loops' measured average sizes are 5.6 nm at 0.3 dpa, 5.4 nm at 1 dpa and 7.4 nm at 2 dpa. The average size at 2 dpa corresponds well to the typical <a>-loop diameters in neutron irradiated Zr alloys of 8 nm stated in the literature [8]. <a>-loops are expected to be of both interstitial and vacancy type [8]; however, the <a>-loop types could not be studied experimentally due to the high loop density and the resulting strong contrasts.

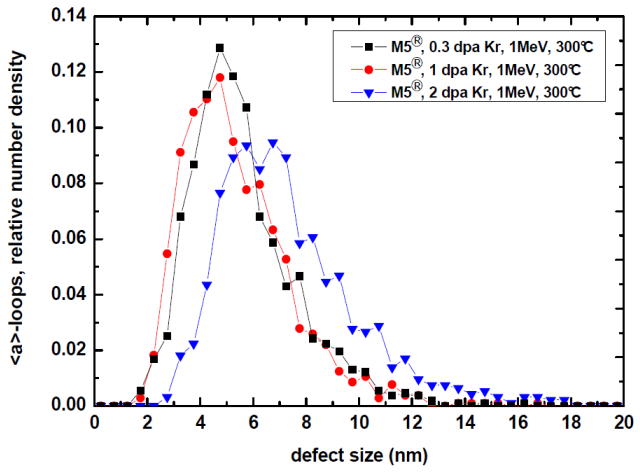

Figure 11: <a>-loop size distribution in sample A1 (1 MeV Kr at 300°C)

3.3.2. <c>-Component Dislocations

The <c>-loop contrast development with the ion dose was studied in one grain of sample A2. An overview TEM picture of the observed grain can be seen in Fig. 12. The grain's diffraction pattern of pole $(2\bar{1}\bar{1}0)$ with the (0002) reflex location is shown next to the BF image. When analyzing in-pile neutron irradiated samples after they received the total neutron dose, it is reported to be difficult to distinguish hydrides oriented parallel to the <c>-loops from the loops. This difficulty is overcome by in-situ TEM, as the hydride distribution in the unirradiated sample is imaged before the irradiation; thus, assuming that the presence of irradiation damage does not influence the hydrogen solubility in the material, all additional line contrasts evolving during irradiation are dislocation loops.

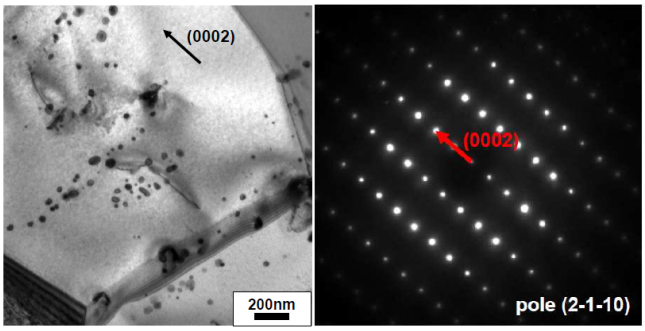

Figure 12: Sample A2, unirradiated grain, $\vec{g}$ = (0002); $(2\bar{1}\bar{1}0)$ pole diffraction pattern

The grains were tested for voids at representative dose levels by alternating over- and underfocus imaging and searching for contrast inversion; from the chosen imaging conditions, voids with a diameter of about 2 nm or higher would have been visible if present in the sample. However, voids were not observed at any dose level. Amorphization of the β-Nb precipitates was not observed; their alternating contrast between bright field and dark field images, and the absence of polycrystal typical rings in the diffraction pattern showed them to be crystalline up to the highest ion dose of 22 dpa. The formation of additional precipitates was not seen during or after irradiation.

The thickness of the grain was determined by imaging a grain boundary parallel to the tilt axis at different tilt angles and measuring the observable grain boundary thickness at these angles. The grain's real thickness can then be calculated from trigonometric relations. The observed grain in sample A2 had a thickness of 181 nm. The measurement error at this method was estimated by calculating the same grain's thickness from different grain boundary thickness measurements; the error showed to be about 10%.

Fig. 13 shows a grain area of sample A2 at a damage level of 22 dpa imaged at a lower magnification to demonstrate that the <c>-loops are homogeneously distributed over the grain. The darker contrast to the right is caused by a more dynamic diffraction condition in that grain region, while the lighter contrast to the left is given by a more kinematical diffraction condition. The difference in the diffraction conditions is due to a slight bending of the grain. Fig. 14 shows the development of the <c>-loops with the ion dose.

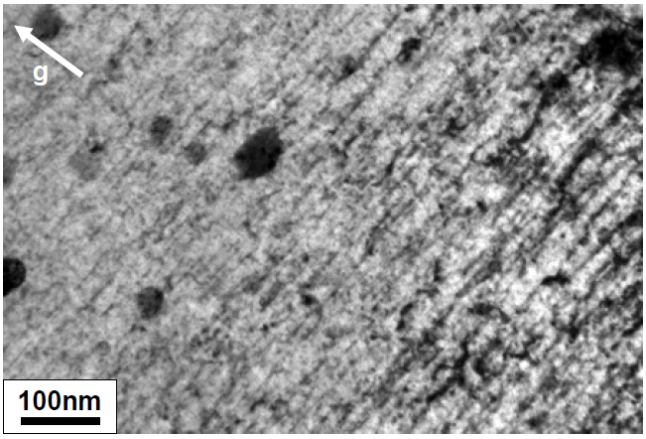

Figure 13: <c>-loop distribution in sample A2 at 22 dpa (1 MeV Kr at 300°C); $\vec{g}$ = (0002)

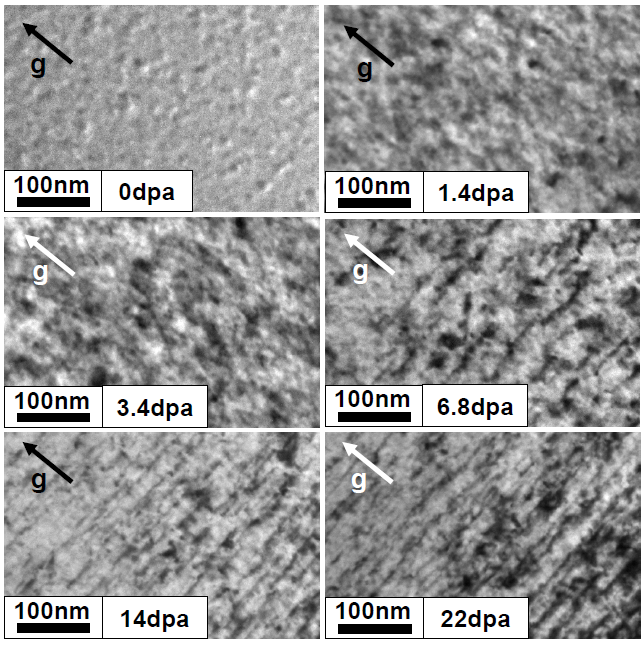

Figure 14: <c>-loop development with the ion dose (1 MeV Kr at 300°C); $\vec{g}$ = (0002)

Contrary to the <a>-loops, <c>-loops are not observed in the early stages of irradiation. Sample A2 was irradiated stepwise; after the step to 6.8 dpa, <c>-loop contrasts were clearly observed, but not in their first state of formation. It can be seen in several of the imaged regions that the <c>-type contrasts are each composed of several smaller contrasts, suggesting small loops that are ordered in a chain-like structure to form the typical line contrast, as indicated by the arrows (see Fig. 15).

To quantitatively determine the loop lengths and densities, the "linear density" is used; it is defined as the sum of the lengths of all <c>-loop contrasts in one image section, divided

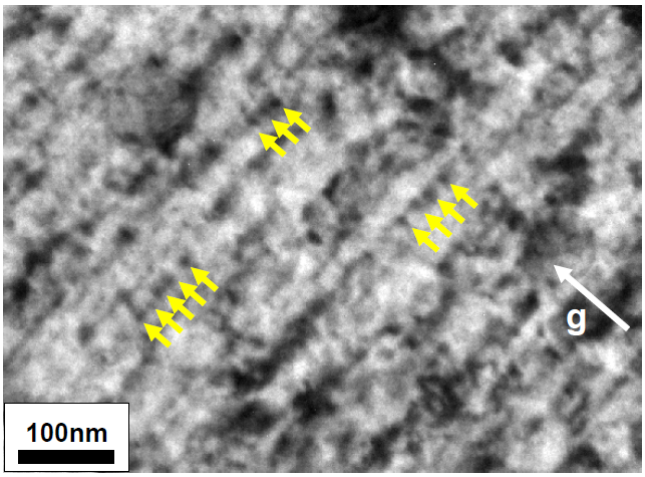

Figure 15: <c>-type contrasts formed by small loops (1 MeV Kr at 300°C); $\vec{g}$ = (0002)

by the imaged material's volume. This is a typical method for the quantification of <c>-loop distributions [11, 37, 46] and has thus been used to compare the measured <c>-loop densities with literature data. For each sample, several grain regions were chosen to determine the linear density from images taken at a magnification of 30'000. The received densities for sample A2 are shown in Fig. 16, together with literature values for heavy ion and neutron irradiated Zr-based alloys [11, 37, 46]. Different symbols for the measured data are used to indicate the different observed positions in the respective grain. A movie was taken for damage levels from 7 dpa to 22 dpa with a higher magnification of 70'000. The higher magnification leads to a visibility of loop contrasts that can not be observed in the lower magnification images; thus, the linear densities measured in frames taken from the movie are higher.

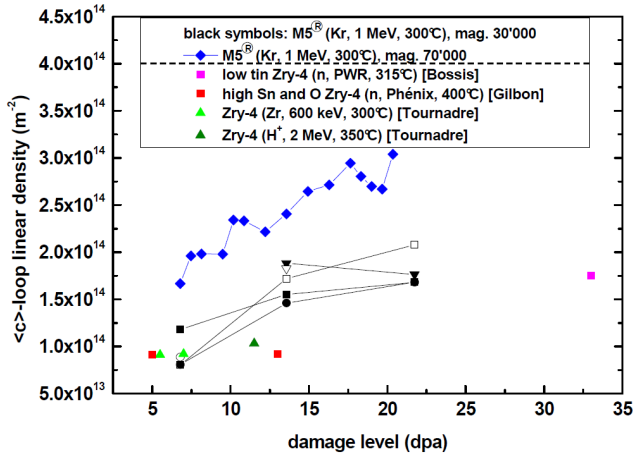

Figure 16: Measured <c>-loop linear densities compared to literature data by Tournadre [11], Bossis [37] and Gilbon [46]

The <c>-loops show an approximately homogeneous distribution over the grains; the statistical variation can be seen by comparing the linear densities calculated from the loop size measurements at different grain positions. A change in the <c>-loop density near outstanding microstructural features like grain boundaries, precipitates or the former hydride location was not observed. It is thus concluded that, if these possible defect sinks have any influence on the <c>-loop formation or behaviour, the effect is not significant under the chosen experimental conditions.

Different literature values for the linear <c>-loop densities have been added to the diagram. As far as the information is contained in the literature, the linear densities were taken from images with magnification of 30'000; thus, the following comparison to literature data is done for the densities measured at 30'000. The ion irradiation induced <c>-loops' linear densities are in good agreement with data on ion irradiated Zircaloy-4 by Tournadre et al. in 2011 [11], for both Zr and proton irradiation. Also, the measured linear densities agree very well with the density reported by Bossis et al. in 2007 for PWR neutron irradiated low tin Zry-4 [37]. They also correspond well to high Sn and O Zry-4 irradiated in the Phénix fast breeder reactor as described by Gilbon et al., 1994 [46].

According to Adamson et al. [47], recrystallized Zircaloys show a three stage growth process; the first stage of growth is small, saturates and is reported to be correlated to <a>-loop formation. The growth rate increases when <c>-loops start to form and is described to be nearly linear with the fluence in ranges that correspond to about 9 to 16 dpa. For higher fluences, the growth rate increases further ("breakaway growth"). As the dose range covered by the described in-situ ion data overlaps with the described linear growth stage, a linear correlation is assumed to fit the development of the linear densities L in sample A2 with the ion dose (see Fig. 17).

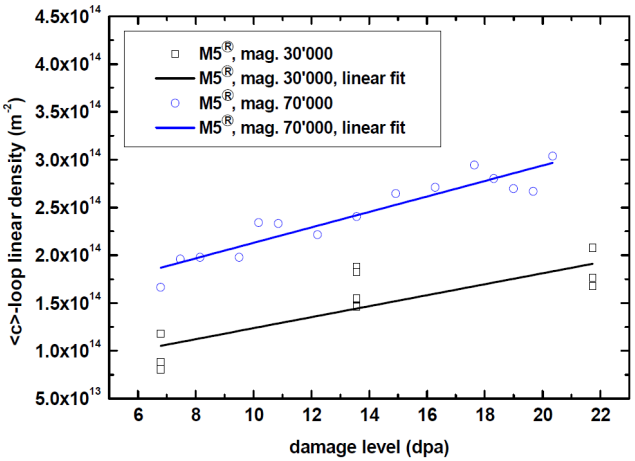

Figure 17: <c>-loop linear density increase with the damage level (1 MeV Kr at 300°C)

The assumed correlation is of the form

$$L_{lin} = L_0 + \dot{L} \cdot D;$$

the fit parameters for the different magnifications are shown in Table 3.

Data	L_0 (m^{-2})	$\dot{L}$ ($m^{-2}dpa^{-1}$)
M5®, mag. 30'000	$(6.6 \pm 2) \cdot 10^{13}$	$(5.7 \pm 1) \cdot 10^{12}$
M5®, mag. 70'000	$(1.3 \pm 0.1) \cdot 10^{14}$	$(8.1 \pm 0.8) \cdot 10^{12}$

Table 3: Fit parameters for the linear densities

As the <c>-loops start to form after a significant dose threshold, their density is zero until that threshold and then increases suddenly as they start to appear; therefore, the assumed linear correlation is only valid for the observed dose range, and not for the dose region of the <c>-loop formation threshold. The images taken with the higher magnification of 70'000 show a higher linear density due to the higher contrast resolution but do also have a 40% higher slope as compared to the densities from the images with magnification 30'000. It can thus be assumed that the density of small <c>-loop contrasts visible only at high magnification increases faster with the damage level than the density of larger loops visible also at lower magnification. This can be an indication that the clustering of small <c>-loops to larger alignments is a slower process than the small <c>-loop formation.

Such a correlation of the <c>-loop linear densities with the dose can be found comparatively fast when using ion irradiation for neutron damage simulation. For neutron irradiation, in-situ TEM imaging is impossible. A comparative study by stepwise in-pile material irradiation takes irradiation times in the range of months or years, and the subsequent TEM preparation can induce preparation artifacts in the samples. Obviously, the imaged material regions would be different after each irradiation step. This shows the huge advantage of the ion simulation method as compared to neutron irradiation, even though it has to be kept in mind that differences in the ion and neutron damage cascades and deviations of the thin TEM foil from the bulk material behaviour might lead to variations in the irradiation damage microstructures.

The <c>-loop size distribution for one position in sample A2 at different damage levels is shown in Fig. 18; Fig. 19 shows the development of the average <c>-loop-size with the ion dose. The error bars shown in Fig. 19 are one standard deviation as a measure of the scattering in length. The average <c>-loop size increases slightly with the dose, from 30.4 nm at 6.8 dpa to 35.6 nm at 22 dpa.

3.3.3. In-situ <c>-loop Annealing

As a complementary measurement to the in-situ defect annealing studied by DBS, a M5® sample irradiated with 1 MeV Kr at 300°C to doses corresponding to 22 dpa was heated up to 750°C to study the development of the <c>-loops with the annealing temperature. The irradiated sample contained, due to an initially different testing purpose, 110 wt.-ppm hydrogen; however, this is considered not to have significant influence on the defect annealing behaviour. After each temperature step, the sample was held at that temperature for about five minutes. The average heating rate during the temperature steps was 7.5 K/min.

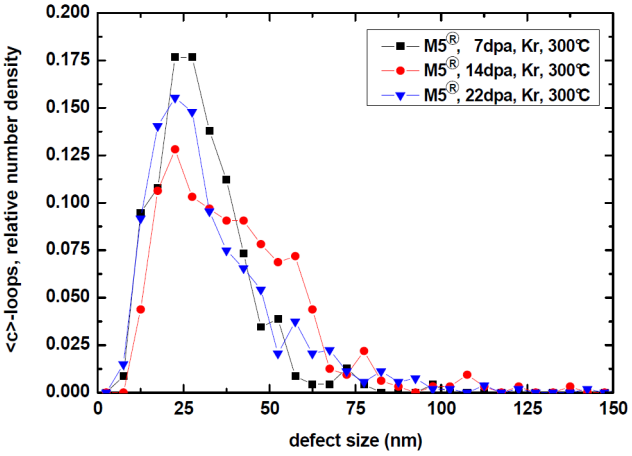

Figure 18: <c>-loop size distribution in ion irradiated M5® (1 MeV Kr at 300°C)

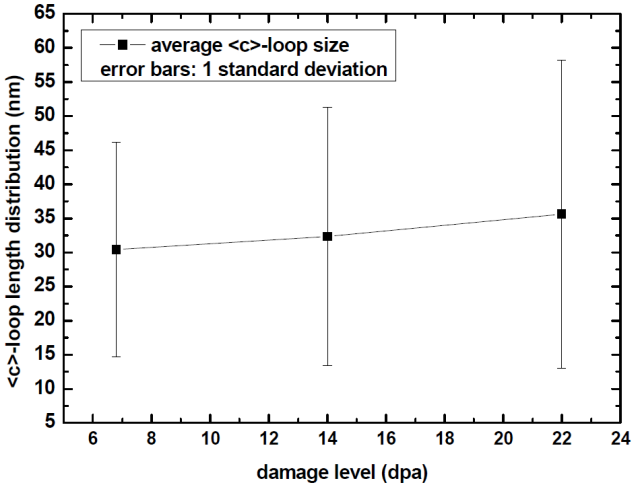

Figure 19: <c>-loop average size distribution in ion irradiated M5® (1 MeV Kr at 300°C)

Fig. 20 shows the <c>-loops in dependence of the annealing temperature, imaged at a magnification of 10'000.

Fig. 21 shows the increase of the average <c>-loop length and the decrease of the loops' number, normalized to the loops' structure at 303°C. The loops' sizes and numbers have been measured three times for the image taken at each temperature; the errors given in the plots are one standard deviation for the average of these three values, corrected for the low number of measurements.

While the DBS measurements described above found a complete annealing of the vacancy-type defects in the irradiated samples at 450°C, the <c>-loops observed during in-situ annealing in the TEM show only a slight tendency of linear density and number decrease and size increase for temperatures lower than 500°C. For temperatures higher than 520°C, the <c>-loops' linear densities and numbers decrease significantly while their length increases; at 750°C, a very low density of

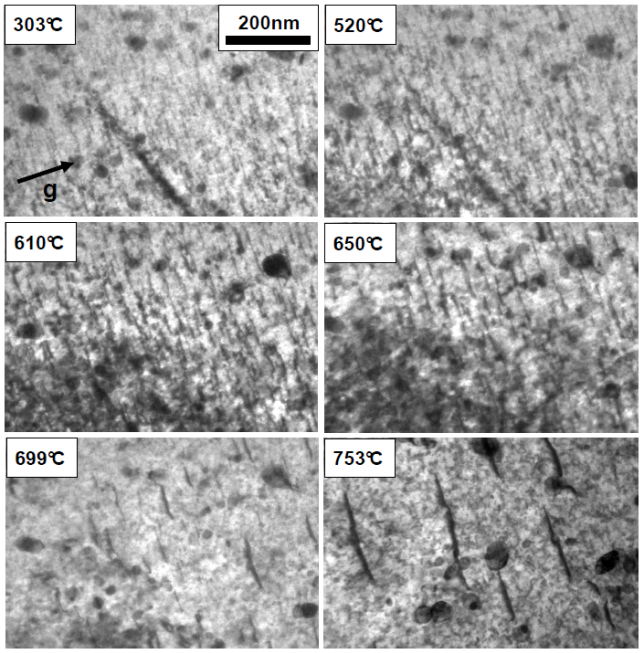

Figure 20: <c>-loop development during annealing (after irradiation with 1 MeV Kr at 300°C)

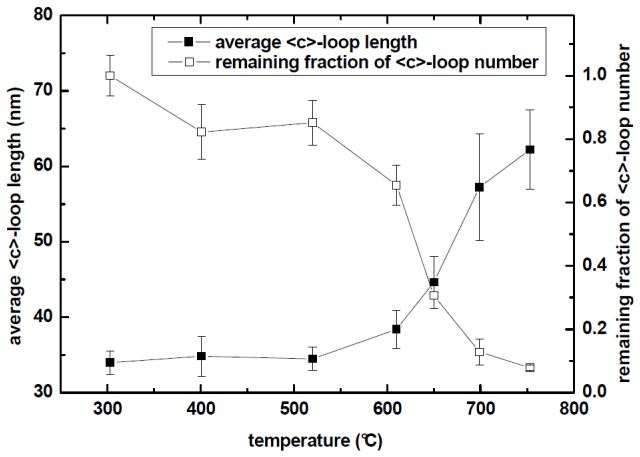

Figure 21: <c>-loop length and number development during annealing (after irradiation with 1 MeV Kr at 300°C)

long <c>-type contrasts remains in the material. For higher temperatures, the contrasts show darker, more even forms, without the short disruptions or kinks that have been observed at lower temperatures. These changes found for higher temperatures suggest that, while a large part of the <c>-loops anneal during the heating process, the remaining chains of small loops transform into dislocation lines.

4. Conclusion

It was shown that heavy ion irradiation in combination with in-situ TEM irradiation damage imaging is an excellent method for the simulation of PWR neutron damage in the Zr-based guide tube alloy M5®. The ion induced irradiation microstructure contains <a>- and <c>-type dislocation loops homogeneously spread over the alloys' grains, with the <a>-loops' sizes and the <c>-loops' linear densities in good agreement with data for neutron irradiated Zr-based alloys. As reported for neutron irradiated Zr-based alloys, the <a>-loops develop from the beginning of the irradiation while the <c>-loops form only above a threshold dose. The comparatively short ion irradiation times allowed to study the development of the <c>-loops' linear densities with the dose up to a dose level of 22 dpa.

Positron Doppler broadening spectroscopy as a complementary method for the study of irradiation damage was used to investigate the dependence of the overall vacancy-type defect density in heavy ion irradiated M5® with the temperature. As expected due to the temperature dependence of the defect mobility, M5® irradiated at 35°C showed a significantly higher defect density than M5® irradiated at 300°C to a considerably higher dose. The overall vacancy-type defect density was completely annealed at 450°C within the resolution limit of DBS. Corresponding TEM analyses of the annealing of <c>-loops up to a temperature of 750°C showed that the <c>-loops' density is too low as compared to the overall vacancy-type defect density to be resolved by DBS. Thus, it can be concluded that the vastly dominating forms of vacancy-type defects in the samples are not present as <c>-loops, but can be expected to be in <a>-loop or mono-vacancy form. During annealing between 520°C and 750°C, the <c>-loops migrate and join to form fewer and larger loops with very strong contrasts that suggest the change from chain-like small loop conglomerates to dislocation lines.

Electron backscatter diffraction was used to measure the penetration depth of 40 MeV Zr in M5®; it was shown that EBSD is sensitive to the ion damage in M5® and that the ion range is in very good agreement to predictions of the SRIM Monte Carlo code. Thus, the application of the code as a basis for the ion dose calculations used in the described experiments is valid.

Acknowledgements

This work was funded by AREVA NP GmbH Corporate Research and Development budget. The IVEM-Tandem Facility (within the Electron Microscopy Center at ANL) is supported by the US DOE Office of Science and operated under contract no. DE - AC02 - 06CH11357 by UChicago Argonne, LLC. The author would like to thank Peter Baldo for the IVEM irradiations, and R.B. Adamson and A.T. Motta for their helpful advice.

M5® is a trade mark of AREVA, registered in France among other countries.

References

[1] D.G. Franklin and R.B. Adamson: "Implications of Zircaloy creep and growth to light water reactor performance", Journal of Nuclear Materials 159 (1988) 12-21

[2] W. Frank: "Intrinsic point defects in hexagonal close-packed metals", Journal of Nuclear Materials 159 (1988) 122-148

[3] D.J. Bacon: "Point defects and clusters in the hcp metals: their role in dose transition", Journal of Nuclear Materials 206 (1993), 249-265

[4] O.T. Woo, G.J.C. Carpenter, S.R. MacEwen: "c-component dislocations in zirconium alloys", Journal of Nuclear Materials 87 (1979), 70-80

[5] C.H. Woo: "Defect accumulation behaviour in hcp metals and alloys", Journal of Nuclear Materials 276 (2000), 90-103

[6] G.J.C. Carpenter, R.A. Murgatroyd, A. Rogerson, J.F. Watters: "Irradiation growth of zirconium single crystals", Journal of Nuclear Materials 101 (1981) 28-37

[7] G.J.C. Carpenter, R.H. Zee, A. Rogerson: "Irradiation growth of zirconium single crystals: a review", Journal of Nuclear Materials 159 (1988) 86-100

[8] G.S. Was: "Fundamentals of Radiation Materials Science", Springer (2007)

[9] R.A. Holt, R.W. Gilbert: "c-component dislocations in annealed zircaloy irradiated at about 570K", Journal of Nuclear Materials 137 (1986), 185-189

[10] R.A. Holt, M. Griffiths, R.W. Gilbert: "c-component dislocations in Zr-2.5wt.%Nb alloy", Journal of Nuclear Materials 149 (1987), 51-56

[11] L. Tournadre, L. Oniumus, D. Gilbon, J.-M. Cloue, J.-P. Mardon, X. Feaugas, O. Toader, C. Bachele: "Experimental Study of Component Loops Nucleation and Growth under Charged Particles Irradiation in Recrystallized Zircaloy-4", TMS Annual Meeting (2011)

[12] C. Abromeit: "Aspects of simulation of neutron damage by ion irradiation", Journal of Nuclear Materials 216 (1994),78-96

[13] A. Sarkar, R. Mukherjee, P. Barat: "Effect of heavy ion irradiation on microstructure of zirconium alloy characterised by X-ray diffraction", Journal of Nuclear Materials 372 (2008), 285-292

[14] A.D. Marwick: "On the simulation of CTR neutron radiation damage by heavy ion irradiation", Journal of Nuclear Materials 56 (1975), 355-358

[15] J.R. Parsons, C.W. Hoelke: "Ion simulation of neutron irradiation growth and creep in Zr and Zr-2,5wt%Nb at 314 K", Journal of Nuclear Materials 114 (1983), 103-107

[16] R.B. Adamson, W.L. Bell, D. Lee: "Use of ion bombardment to study irradiation damage in zirconium alloys", Zirconium in Nuclear Applications, ASTM STP 551, American Society for Testing and Materials (1974) pp. 215-228

[17] R.M. Hengstler, L. Beck, H. Breitkreutz, C. Jarousse, R. Jungwirth, W. Petry, W. Schmid, J. Schneider, N. Wieschalla: "Physical properties of monolithic U8wt.-%Mo", Journal of Nuclear Materials 402, 74-80 (2010)

[18] N. Wieschalla, A. Bergmaier, P. Böni, K. Böning, G. Dollinger, R. Großmann, W. Petry, A. Röhrmoser, J. Schneider: "Heavy ion irradiation of U-Mo/Al dispersion fuel", Journal of Nuclear Materials 357, 191-197 (2006)

[19] G.J.C. Carpenter, J.F. Watters: "A study of electron irradiation damage in zirconium using a high voltage electron microscope", Journal of Nuclear Materials 96, 213-226 (1981)

[20] S.N. Buckley, S.A. Manthorpe: "Dislocation loop nucleation and growth in Zirconium-2.5wt%Niobium alloy during 1MeV electron irradiation", Journal of Nuclear Materials 90, 169-174 (1980)

[21] M. Griffiths, M.H. Loretto, R.E. Smallman: "Electron damage in Zirconium - I. Defect structure and loop character", Journal of Nuclear Materials 115, 313-322 (1983)

[22] M. Griffiths, M.H. Loretto, R.E. Smallman: "Electron damage in Zirconium - II. Nucleation and growth of c-component loops", Journal of Nuclear Materials 115, 323-330 (1983)

[23] L. Fournier, A. Serres, Q. Auzoux, D. Leboulch, G.S. Was: "Proton irradiation effect on microstructure, strain localization and iodine-induced stress corrosion cracking in Zircaloy-4", Journal of Nuclear Materials 384, 38-47 (2009)

[24] X.T. Zu, K. Sun, M. Atzmon, L.M. Wang, L.P. You, F.R. Wan, J.T. Busby, G.S. Was, R.B. Adamson: "Effect of proton and Ne irradiation on the microstructure of Zircaloy 4", Philosophical Magazine, Vol. 85, Nos. 4-7, 649-659 (2005)

[25] C.W. Allen, L.L. Funk, E.A. Ryan: "New instrumentation in Argonne's HVEM-Tandem Facility: Expanded capability for in-situ beam studies", Mat. Res. Soc. Symp. 396: 641-646 (1996)

[26] P. Pikart, C. Hugenschmidt, J. Mayer, M. Stadlbauer, K. Schreckenbach: "Depth resolved Doppler broadening measurement of layered Al-Sn samples", Applied Surface Science 255 (2008), 245-247

[27] C. Hugenschmidt, J. Mayer, M. Stadlbauer: "Investigation of the near surface region of chemically treated and Al-coated PMMA by Doppler-broadening spectroscopy", Radiation Physics and Chemistry 76 (2007), 217-219

[28] T. Iwai, H. Tsuchida, M. Awano: "Application of positron beam Doppler broadening technique to ion beam irradiation in Nickel", Journal of Nuclear Materials 367-370 (2007), 372-376

[29] C. Zhou, X. Liu, C. Ma, B. Wang, Z. Zhang, L. Wei: "Positron beam studies of irradiated polycrystal α-Zr", Journal of Applied Physics 97 (2005), 063511

[30] C. Hugenschmidt, K. Schreckenbach, M. Stadlbauer, B. Straßer: "Low energy positrons of high intensity at the new positron beam facility NEPOMUC", Nuclear Instruments and Methods in Physics Research A 554 (2005), 384-391

[31] C. Hugenschmidt, G. Dollinger, W. Egger, G. Kögel, B. Löwe, J. Mayer, P. Pikart, C. Piochacz, R. Repper, K. Schreckenbach, P. Sperr, M. Stadlbauer: "Surface and bulk investigations at the high intensity positron beam facility NEPOMUC", Applied Surface Science 255 (2008), 29-32

[32] M. Stadlbauer, C. Hugenschmidt, K. Schreckenbach, P. Böni: "Investigation of the chemical vicinity of crystal defects in ion-irradiated Mg and a Mg-Al-Zn alloy with coincident Doppler broadening spectroscopy", Physical Review B 76, 174104 (2007)

[33] J.F. Ziegler: "www.srim.org" (2011)

[34] H. Okamoto: "Nb-Zr (Niobium-Zirconium)", Journal of Phase Equilibria 13, No.5 (1992)

[35] D. Baron, I. Arimescu, G. Shimanski, L. Hallstadius, S. Yagnik: "The NFIR-V Dimensional Stability Project: A Method for Transposing Test Reactor Irradiation Data for PWR and BWR Applications", EPRI, Palo Alto, CA: 2009.1019098 (2009)

[36] J.V.N. Shishov, A.V. Nikulina, M.M. Pergud, V.F. Kon'kov, V.V. Novikov, V.A. Markelov, T.N. Khokhunova, G.P. Kobylyansky, A.E. Novoselov, Z.E. Ostrovsky, A.V. Obukhov: "Structure-phase state, corrosion and irradiation properties of Zr-Nb-Fe-Sn system alloys", 15th symposium "Zirconium in the Nuclear Industry"(2007), ASTM STP 1505

[37] P. Bossis, B. Verhaeghe, S. Doriot, D. Gilbon, V. Chabretou, A. Dalmais, J.P. Mardon, M. Blat, A. Miquet: "In PWR Comprehensive Study of High Burn-up Corrosion and Growth Behavior of M5® and Recrystallized Low-Tin Zircaloy-4", Zr in the Nuclear Industry: 15th International Symposium (2007)

[38] J.-P. Mardon, D. Charquet, J. Senevat: "Influence of composition and fabrication process on out-of-pile and in-pile properties of M5 alloy", Zirconium in the Nuclear Industry: 12th International Symposium (2000), ASTM STP 1354

[39] W. Zhou, Z.L. Wang: "Scanning Microscopy for Nanotechnology. Techniques and Applications", Springer Science+Business Media, LLC (2007)

[40] D.B. Williams, C.B. Carter: "Transmission Electron Microscopy. A Textbook for Materials Science", Springer Science+Business Media, LLC (2009)

[41] C. Hugenschmidt, B. Löwe, J. Mayer, C. Piochacz, P. Pikart, R. Repper, M. Stadlbauer, K. Schreckenbach: "Unprecedented intensity of a low-energy positron beam", Nuclear Instruments and Methods in Physics Research A 593 (2008) 616-618

[42] M. Stadlbauer, C. Hugenschmidt, K. Schreckenbach: "New design of the CDB-spectrometer at NEPOMUC for T-dependent defect spectroscopy in Mg", Applied Surface Science 255 (2008) 136-138

[43] M. Haaks: "M Spec 2: http://agmaier.hiskp.uni-bonn.de/en/material_science/software/mspec_2.html" (2011)

[44] M.J. Puska, R.M. Nieminen: "Theory of positrons in solids and on solid surfaces", Reviews of Modern Physics, Vol. 66, No. 3 (1994)

[45] G.M. Hood, R.J. Schultz, J.A. Jackman: "The recovery of single crystal α-Zr from low temperature electron irradiation-a positron annihilation spectroscopy study", Journal of Nuclear Materials 126 (1984) 79-82

[46] D. Gilbon, C. Simonot: "Effect of irradiation on the microstructure of Zry-4", Zr in the Nuclear Industry: 10th International Symposium, ASTM STP 1245 (1994)

[47] R. Adamson, F. Garzarolli, C. Patterson: "In-reactor creep of zirconium alloys", Advanced Nuclear Technology International, www.antinternational.com (2009)